metals

MDPI

Article

In Vitro Bone Cell Behavior on Porous Titanium Samples: Influence of Porosity by Loose Sintering and Space Holder Techniques

Ana Civantos [1,*], Mercè Giner [2,*], Paloma Trueba [3], Sheila Lascano [4], María-José Montoya-García [5], Cristina Arévalo [3], María Ángeles Vázquez [5], Jean Paul Allain [1,6] and Yadir Torres [3]

1 Department of Nuclear, Plasma and Radiological Engineering, College of Engineering, University of Illinois at Urbana-Champaign, Urbana 61801, IL, USA; allain@psu.edu
2 Departamento de Citología e Histología Normal y Patológica, Universidad de Sevilla, Avda. Dr.Fedriani s/n, 41009 Sevilla, Spain
3 Departamento de Ingeniería y Ciencia de los Materiales y del Transporte, Escuela Politécnica Superior, Calle Virgen de África 7, 41011 Seville, Spain; ptrueba@us.es (P.T.); carevalo@us.es; carevalo@us.es (C.A.); ytorres@us.es (Y.T.)
4 Departamento de Ingeniería Mecánica, Universidad Técnica Federico Santa María, Avda. Vicuña Mackenna 3939, Santiago de Chile 8940000, Chile; sheila.lascano@usm.cl
5 Medicine Department, University of Seville, Avda. Dr. Fedriani s/n, 41009 Sevilla, Spain; pmontoya@us.es (M.-J.M.-G.); mavazquez@us.es (M.Á.V.)
6 The Ken and Mary Alice Lindquist Department of Nuclear Engineering, Pennsylvania State University, State College 16802, PA, USA
* Correspondence: ancife@illinois.edu (A.C.); mginer@us.es (M.G.); Tel.: +217-766-0951 (A.C.); +34-627-217-746 (M.G.)

Received: 15 April 2020; Accepted: 19 May 2020; Published: 25 May 2020

Abstract: A great variety of powder metallurgy techniques can produce biomimetic porous titanium structures with similar mechanical properties to host bone tissue. In this work, loose sintering and space holder techniques, two frequently used metallurgical techniques, are compared to evaluate the influences of porosity (content, size, morphology and wall roughness), mechanical properties (stiffness and yield strength) and in-vitro cellular responses (adhesion and proliferation of myoblasts and osteoblasts). These comparisons are made to achieve the best balance between biomechanical and bifunctional behavior of a partial porous implant for cortical bone replacement. Cell adhesion (filopodia presence) and spreading were promoted on both porous surfaces and fully dense substrates (non-porous control surfaces). Porous scaffold samples designed using 50 vol.% NaCl space holder technique had an improved bioactive response over those obtained with the loose sintering technique due to higher roughness and scaffold pore diameter. However, the presence of large and heterogeneous pores compromises the mechanical reliability of the implant. Considering both scenarios, the substrates obtained with 40 vol.% NH_4HCO_3 and pore size ranges between 100 and 200 μm provide a balanced optimization of size and strength to promote in-vitro osseointegration.

Keywords: porous titanium; space holder; loose sintering; mechanical behavior; cell adhesion; surface roughness

1. Introduction

For many decades, the emphasis of human biomechanics has been on the partial or total replacement of bone tissue with synthetic implants that the body will, in time, integrate as functional parts. Clinical success is achieved when the osteoimplant maximizes the osseointegration and

regeneration of the bone, improving patient health quality. The strategy is for the osteoimplant to provide structural support while reproducing the original stress/strain functionality of the patient's bone under normal usage. Among all other metallic biomaterials used for bone replacement, titanium (Ti) and its alloys have been recognized as the materials with the best in-vivo and in-vitro performance due to their high mechanical strength, fracture toughness, good corrosion resistance and excellent biological properties [1–7], such as biocompatibility and osteoconductivity (the ability to grow bone tissues over the scaffold surface) [8–10]. However, these materials have shown important drawbacks that compromise the reliability of implants: stress-shielding phenomena [11–13] and poor osseointegration [14,15]. The stress-shielding effect is caused by the stiffness mismatch between the implant and the surrounding bone (105–110 GPa vs. 2–25 GPa) [16,17]. As a consequence, the implant does not transfer the entire applied load to the bone, which finally promotes bone resorption and implant loosening [18]. In addition, the inert biological character of titanium surfaces results in a poor cellular interaction between Ti and host bone tissue—an outcome that can affect the proper reconstruction of bone, resulting in chronic failure of the implant [19]. For these reasons, the development of a biofunctional Ti implant with enhanced osseointegration for bone tissue replacement remains a challenge to be addressed.

The design and manufacturing of implants with lower stiffness are presented as a solution to stress shielding [20–22] and several preliminary efforts have been carried out to achieve implants with a suitable balance between mechanical and biofunctional behavior [23–27]. The reduction of the implant Young's modulus can be addressed by the design of a porous architecture for titanium-based systems. Among the fabrication options for porous titanium, loose sintering (LS) and space holder (SH) techniques have been identified as low-cost routes [28,29]. However, both techniques result in different porous titanium substrates in terms of mechanical properties and pore design, key factors in bone-implant integration.

Furthermore, it is well-known that bone ingrowth with porous structures can vary with the specific pore size of the porous material. Osteoblastic cells are able to attach and produce bone matrix inside pores that preferentially present at least a 100 μm average pore size [26,29]. The introduction of porosity and a rough surface into a biomaterial broadens the scope for possible applications in the biomedical field, because the roughness, higher surface contact and surface free energy have been considered important factors that affect cell adhesion, migration and differentiation [30]. It has been reported that the pores obtained by the space-holder technique and loose sintering have an intrinsic surface roughness, which improves the cell adhesion and inhibits the bacterial attachment [31,32]. Although rough and porous surfaces have positively influenced the fixation and long-term stability of Ti implants [20,33–36], finding the right balance between Young's modulus and cell interaction remains elusive. Therefore, an excellent approach to improve the reliability of titanium implants and increase clinical success is to design porous titanium implants with an equilibrium of mechanical properties and favorable bioactivity of titanium porous materials [37,38].

In our group, the influences of the spacer particle content (NaCl) on mechanical properties and pore geometry have been studied before [24,39] and we have made a comparison with the LS technique [26]. In addition, the cellular responses of macrophages and osteoblast growing on NH_4HCO_3 porous scaffolds have been also evaluated, including a chemical surface modification, but limited knowledge is related to the in-vitro cellular response to LS and SH porous substrates. In that sense, we have not investigated the comparison of pore size and morphology, or the effects from total and interconnected porosity that both powder metallurgy (PM) routes have on cell responses.

In this work, porous titanium samples obtained by two different powder metallurgy routes (LS, and SH) were fabricated. The influences of content, size range, surface roughness and morphology of the porosity on the mechanical behavior (stiffness and yield strength), and cell adhesion and proliferation, were investigated in detail.

2. Materials and Methods

Commercially pure titanium (c.p. Ti) powder produced by a hydrogenation/dehydrogenation process has been used as the starting powder (SE-JONG Materials Co. Ltd., Incheon, Korea). The

titanium powder was equivalent to c.p. Ti Grade IV (ASTM F67-00). Sodium chloride, NaCl (Panreac Química S.A.U., Barcelona, Spain, purity > 99.5%), and ammonium bicarbonate, NH_4HCO_3 (Cymit Química S.L, Barcelona, Spain, with a purity of 99.9%) were employed as spacers. Two routes were implemented to obtain porous titanium samples: (1) conventional powder metallurgy with no applied pressure (loose sintering, LS) and (2) space-holder technique (SH) with different content and size range of spacer particles. The particle size distributions and the main aspects of the manufacturing routes are summarized in Table 1.

In the LS technique, the Ti powder was poured and vibrated into a cylindrical mold of alumina for 2 min and then sintered in a CARBOLYTE STF (Derbyshire, UK) 15/75/450 ceramic furnace with a horizontal tube at two different temperatures (1000 and 1100 °C), for 2 h, under high vacuum conditions (~10^{-5} mbar). On the other hand, in the SH route, the mixture of c.p. Ti powder and space-holder particles (NaCl and NH_4HCO_3) was homogenized using a Turbula® T2C mixed for 40 min [39,40]. Then the mixture was pressed at 800 MPa in an INSTRON 5505 machine (Instron, MA, USA). Afterward, the elimination of the NaCl spacer was carried out by dissolution on distilled water [39] and removed by thermal evaporation in the case of NH_4HCO_3 [40]. Finally, the samples were sintered in these cases at 1250 °C, during 2 h and under high vacuum conditions (~10^{-5} mbar).

Table 1. Manufacturing parameters of porous titanium cylinders.

Route			Size Distribution, d[10], d[50], d[90] (μm)		Compaction Pressure (MPa)	Spacer Removal Procedure	Sintering Temperature (°C)
			Titanium Powder	Spacer Particles			
Loose Sintering				None	0	None	1000 1100
Space Holder	NaCl	30 vol.%	9.7, 23.3, 48.4	183, 384, 701	800	Distilled water, without stirring, 50 °C, during 16 h	1250
		50 vol.%					
	NH_4HCO_3	30 vol.%		73, 233, 497		Two steps: 60 °C and 110 °C. Both in low vacuum conditions (~10^{-2} mbar) and 12 h	
				100-200			
		40 vol.%		119, 184, 286			
				355-500			
				355, 424, 564			

2.1. Microstructural and Macro-Mechanical Behavior

The porosity and mechanical properties of porous Ti samples were characterized using different techniques (at least three specimens have been tested in all cases): (1) Archimedes' method (ASTM C373-88) which allows the evaluation of the density, and the total and interconnected porosity (P_T and P_i, respectively). (2) Image analysis (IA), performed with an optical microscope Nikon Epiphot (Nikon, Tokyo, Japan) coupled with a Jenoptik Progres C3 camera (Jenoptik, Jena, Germany), and processed in the software Image-Pro Plus 6.2, Mediacibernetic, Bethesda, MD, USA. IA was evaluated with 10 pictures of 5× and 20× for each processing condition. This technique provides the analysis of (i) the total porosity percentage (P_{IA}), (ii) equivalent diameter (D_{eq}) and (iii) pore shape factor (F_f). (3) The uniaxial compression test (Standard ASTM E9-89A and ISO 13314: 2011) allowed the determination of yield strength (σ_y) and Young's modulus (E_c). (4) The ultrasound technique, which was used to study the dynamic Young's modulus (E_d) [40,41].

2.2. In-Vitro Cell Experiments

In order to study the cell viability, adhesion, proliferation and cell morphologies of myoblast and osteoblasts growing in the different porous substrates, cross-sections were prepared from the titanium porous cylinders. The different tests and techniques used to evaluate cellular response, are described in the following scheme—Figure 1.

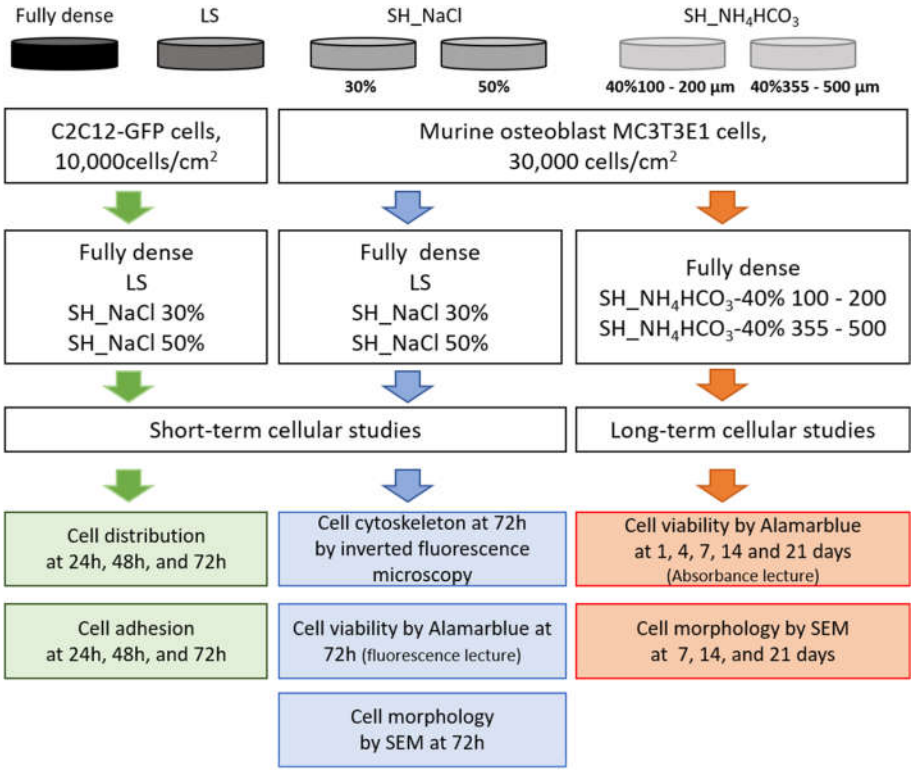

Figure 1. Diagram of in-vitro experimental design. Two murine cell lines, myoblasts (C2C12-GFP) and osteoblasts (MC3T3E1) were used to analyze the biological response to c.p. Ti fully dense and porous substrates.

2.1.1. Cell Adhesion and Proliferation of Myoblast Cells

C2C12 cell line (mouse myoblast cell line, CRL-1772 obtained from American Type Culture Collection, ATCC, Manassas, VA, USA) was used to follow cell adhesion and proliferation processes on porous titanium samples. This cell line was transfected previously to constitutively express GFP (green fluorescent protein); thus, samples were evaluated by inverted fluorescent microscope. Cells passaged were carry out using Dulbecco's modified eagle's medium (DMEM) supplemented with 10% of fetal bovine serum (FBS) plus antibiotics (100 U/mL penicillin and 100 mg/mL streptomycin sulfate) (Invitrogen). Samples were sterilized in an autoclave and placed in a 24-well plate, seeded with 10,000 cells /cm^2. After 24, 48 and 72 h of incubation, samples were inverted to observe the presence of cells (green fluorescence) attached to the bottom on each well and the porous surfaces using an inverted fluorescent microscope (Olympus IX51).

2.1.2. In-Vitro Evaluation of Osteoblast Response

MC3T3E1, a murine pre-osteoblast cell line (CRL-2593, from ATCC, Manassas, VA, USA), was utilized to analyze the porosity's effect on cell metabolism and viability during cell adhesion and proliferation process. Routine passaging of the cell line was performed on 25 cm^2 flasks with minimum essential medium (MEM), containing 10% fetal bovine serum plus antibiotics (100 U/mL penicillin and 100 mg/mL streptomycin sulfate) (Invitrogen). Autoclaved porous titanium samples were carefully placed into a 24-well plate, and trypsinized osteoblasts cells were seeded at a cellular density of 30,000 cells/cm^2 per sample. Afterward, 800 µL of prewarmed culture medium was added,

and culture plates were kept at 37 °C in a humidified 5% CO_2 atmosphere. Triplicate blank and TCP (tissue culture plastic) were used as negative and positive controls in the same plate for each time period. Two types of in-vitro experiments were tested: (i) short time experiments to evaluate cell adhesion, proliferation and morphology at 24, 48 and 72 h, and (ii) long-term studies to analyze the cell proliferation and cell morphology of differentiated osteoblasts. These latter experiments were carried out at 1, 4, 7, 14 and 21 days of culturing osteoblasts with osteogenic media (α-MEM medium supplemented with 10 mM ascorbic acid (Merck, Germany) and β-glycerophosphate (StemCell Technologies, Vancouver, BC, Canada) 50 μg/mL). For the evaluation of cell viability and metabolism of osteoblast, AlamarBlue® reagent (Invitrogen, Waltham, MA, USA) was selected. Briefly, at the end of each culture period, samples were collected to a new 24-well plate to avoid counting non-attached or attached cells on the well plate. New fresh media (800 μL) and 80 μL of AlamarBlue® reagent were added and the plate was incubated during 1 h 30 min at 37 °C in dark conditions. After that, samples were removed and culture medium was read by fluorescence signal (Biotek FL-600) and absorbance at 570 nm (TECAN, Infinity 200 Pro) for short and long-term studies, respectively. Cell differentiation studies based on alkaline phosphatase (ALP) enzyme quantification were analyzed according to the manufacturer's protocol (Alkaline Phosphatase Assay kit Colorimetric, Abcam ab83369, Cambridge, UK) of osteoblast cultured on osteogenic media at 4 and 21 days. Basically, ALP kit measures the conversion of a colorless p-nitrophenyl phosphate to a colored p-nitrophenol and the lecture of the absorbance at 405 nm is measured in a 96-well microplate reader. The ALP activity was calculated from a standard curve also measured in the same plate at the same time. Cytoskeletal organization was studied at 72 h using Texas red phalloidin (Molecular Probes) and Hoechst (Thermofisher) as a contrast staining for cell nuclei. In short, cells were rinsed twice with PBS, fixed in 4% paraformaldehyde and permeabilized in 0.1% buffered Triton X-100, and 5 μL/mL from a solution of actin (Texas Red Pahlloidin) in PBS was used for visualization the F-actin for 20 min. After the incubation period, samples were washed with PBS, and images were obtained in an Olympus IX51 microscope. DAPI staining was used to quantify cell nuclei using ImageJ 2.0. software (National Institutes of Health and the Laboratory for Optical and Computational Instrumentation (LOCI, University of Wisconsin, Madison, WI, USA). Finally, scanning electron microscopy (SEM) was performed to evaluate the cell morphology at short (1, 2 and 3 days) and long-term points (7, 14 and 21 days). The samples were fixed in 10% formalin, followed by a dehydration step with ethanolic solutions and coated by gold-coating using a sputter coater (Pelco 91000, Ted Pella, Redding, CA, USA). All micrographs were obtained using a Jeol JSM-6330F scanning electron microscope (Jeol, Tokyo, Japan), and the acceleration voltage was 10 kV for SEM images.

2.1.3. Statistical Analysis

All in-vitro experiments were performed in triplicate, with n = 3 for each studied condition. Results were expressed as means and standard deviations to perform a two-way ANOVA followed by a Tukey's post-test using OriginPro 2019 software (OriginLab, Northampton, MA, USA). Significance was considered at p values of $p < 0.05$ (*) and $p < 0.01$ (**).

3. Results

Significant progress has been made toward the development of porous c.p. titanium scaffolds for orthopedic and dental applications. Two different porous titanium routes (LS and SH) and two spacer holder particles (NaCl and NH_4HCO_3) were tested to evaluate their influences on the development of porous scaffolds with suitable porosity and mechanical properties. These sintering routes were performed following the Materials and Methods' description and the ASTM and ISO guidelines.

3.1. Porosity and Mechanical Behavior

Table 2 shows Archimedes' method, image analysis, the compression test and ultrasonic technique results from the samples fabricated using both routes (LS and SH) and different

manufacturing conditions (see Table 1). The porosity evaluation was studied in detail. A representation of the values from both methods is shown in Figure 2.

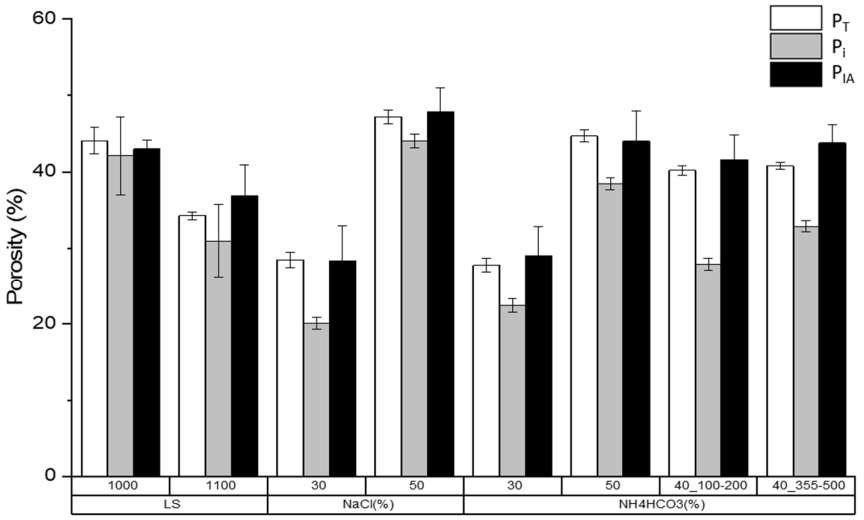

Figure 2. Comparative analysis of the porosity values (P_T, P_i and P_{IA}) found in LS and SH porous Ti substrates. The highest porosity values were found in the 50 vol.% NaCl porous substrates.

The resultant porosity (P_{IA}) by IA was similar to the values obtained by Archimedes' method. Total porosity achieved by the LS route was lower when the temperature was increased (P_T = 44.1% at 1000 °C, and P_T = 34.3% at 1100 °C). On the other hand, for the SH route, the porosity values found in NaCl were higher, despite the fact it was the same content of spacer as in NH_4HCO_3 (i.e., for 30 vol.% of NaCl, the P_T was 28.5% versus the same percentage, 30 vol.%, of NH_4HCO_3 that had a P_T of 27.8%). This effect was also observed in 50 vol.% of both porous substrates which is explained by the space-holder particle size (see Table 1).

Concerning the topographical parameters of the designed porosity, the results demonstrate that: (1) The equivalent diameter (D_{eq}) was increased when the temperature and/or spacer content increased. This result is associated with the pore coalescence. Additionally, the values of equivalent diameter are consistent with the average sizes of the spacers used. (2) The pore sizes found in SH samples do not allow bone growth towards the interior of the implant, >100 μm being the size reference. (3) The pore size factor (F_f) parameter is a measure of the roundness of the pores (greater when are closer to 1.0). In general, these are greater when the SH method is used. The roundness increases with the sintering temperature (decreases the surface tension), while an increase of the spacer content generates more irregular pores.

Regarding the mechanical behavior, the values from the elastic limit and Young's modulus are consistent with the contents and pore sizes fabricated. In this context, larger pores and in greater proportion decrease yield strength and stiffness, respectively. The loss of mechanical resistance may also be related to the poor quality of the sintering necks (both for low compaction pressures and temperatures) and the increase of the stress concentrator in more irregular pores. Moreover, the reliability of mechanical behavior depends on the population width of the spacer size; it is noted that this generally increases for narrower populations. In general, in samples obtained with 40 vol.% NH_4HCO_3 and range size of 100–200 μm, obtained by SH (235 MPa and 45.3 GPa), provide a better scenario for the replacement of cortical bone (σ_y = 150–180 MPa and E = 20–25 GPa).

Table 2. Values obtained from Archimedes' method, image analysis (IA) and estimated mechanical behavior.

Physical and Mechanical Properties		Loose Sintering		Space Holder					
				NaCl		NH_4HCO_3			
							40 (vol. %)		
		1000°C	1100°C	30 (vol.%)	50 (vol.%)	30 (vol.%)	100–200 μm	355–500 μm	50 (vol.%)
Archimedes' method	P_T (%)	44.1 ± 1.7	34.3 ± 0.5	28.5 ± 1.0	47.2 ± 0.9	27.8 ± 0.9	40.2 ± 0.6	40.8 ± 0.5	44.7 ± 0.8
	P_i (%)	42.1 ± 5.1	31.0 ± 4.8	20.5 ± 0.8	44.1 ± 0.9	22.4 ± 0.9	27.9 ± 0.8	32.9 ± 0.7	38.5 ± 0.8
	Density (g/cm^3)	2.5 ± 0.2	2.8 ± 0.2	3.2 ± 0.2	2.2 ± 0.2	3.6 ± 0.2	2.69 ± 0.02	2.67 ± 0.02	2.50 ± 0.2
Image analysis	P_{IA} (%)	43.0 ± 1.2	36.9 ± 4.0	28.4 ± 4.6	47.9 ± 3.1	29.1 ± 3.8	41.6 ± 3.3	43.8 ± 2.4	44.0 ± 4.0
	D_{eq} (μm)	16 ± 17	19 ± 16	370 ± 244	392 ± 260	230 ± 202	226 ± 178	295 ± 287	245 ± 223
	F_f	0.76 ± 0.11	0.85 ± 0.09	0.81 ± 0.13	0.70 ± 0.14	0.83 ± 0.11	0.71 ± 0.12	0.67 ± 0.06	0.79 ± 0.08
Uniaxial Compression	E_c (GPa)	13.4 ± 6	21.0 ± 4	6.6 ± 5	5.2 ± 5.0	15.9 ± 4.1		-	8.5 ± 7.0
	σ_y (MPa)	128 ± 6	206 ± 5	323 ± 10	117 ± 12	298 ± 8	235 ± 6	190 ± 5	149 ± 9
Ultrasound	E_d (GPa)	42.2 ± 1.0	52.1 ± 1.2	58.9 ± 0.9	39.5 ± 1.3	59.8 ± 1.2	45.9 ± 0.7	45.3± 0.8	41.7 ± 1.0

3.2. Cell Adhesion and Proliferation

Porous titanium samples fabricated by LS and SH result in a variety of reduced Young´s moduli as a function of porosity size and distribution (interconnected, total and pore density). It is well-known that surface parameters affect the cell interactions at the bio-interface. Therefore, the study of cellular response correlated to the mechanical properties of porous titanium should be assessed.

First, porous c.p. Ti substrates were seeded with C2C12-GFP cells in order to evaluate cell adhesion, distribution and proliferation during 24–72 h of cell incubation; see Figure 3. Images of fluorescence microscopy were taken every day to compare the main differences in cell growth in fully dense, LS and SH (30 vol.% and 50 vol.% NaCl) substrates. It can be observed that C2C12-GFP cells were attached in all titanium substrates at 24 h. The cell density increased over time, highlighting the suitable biocompatibility of both sintering porous routes. These micrographs demonstrated differences in cell distribution that were even noticeable at 24 h of study. A fully dense surface presented a dense cellular monolayer located in the center of the sample. Cells growing on LS and SH substrates were highly disperse, covering almost the entire surface area. This cell behavior was highlighted at 72 h of cell proliferation in which an increased cell density was reached on LS and SH_50%NaCl surfaces compared to SH_30%NaCl and fully dense.

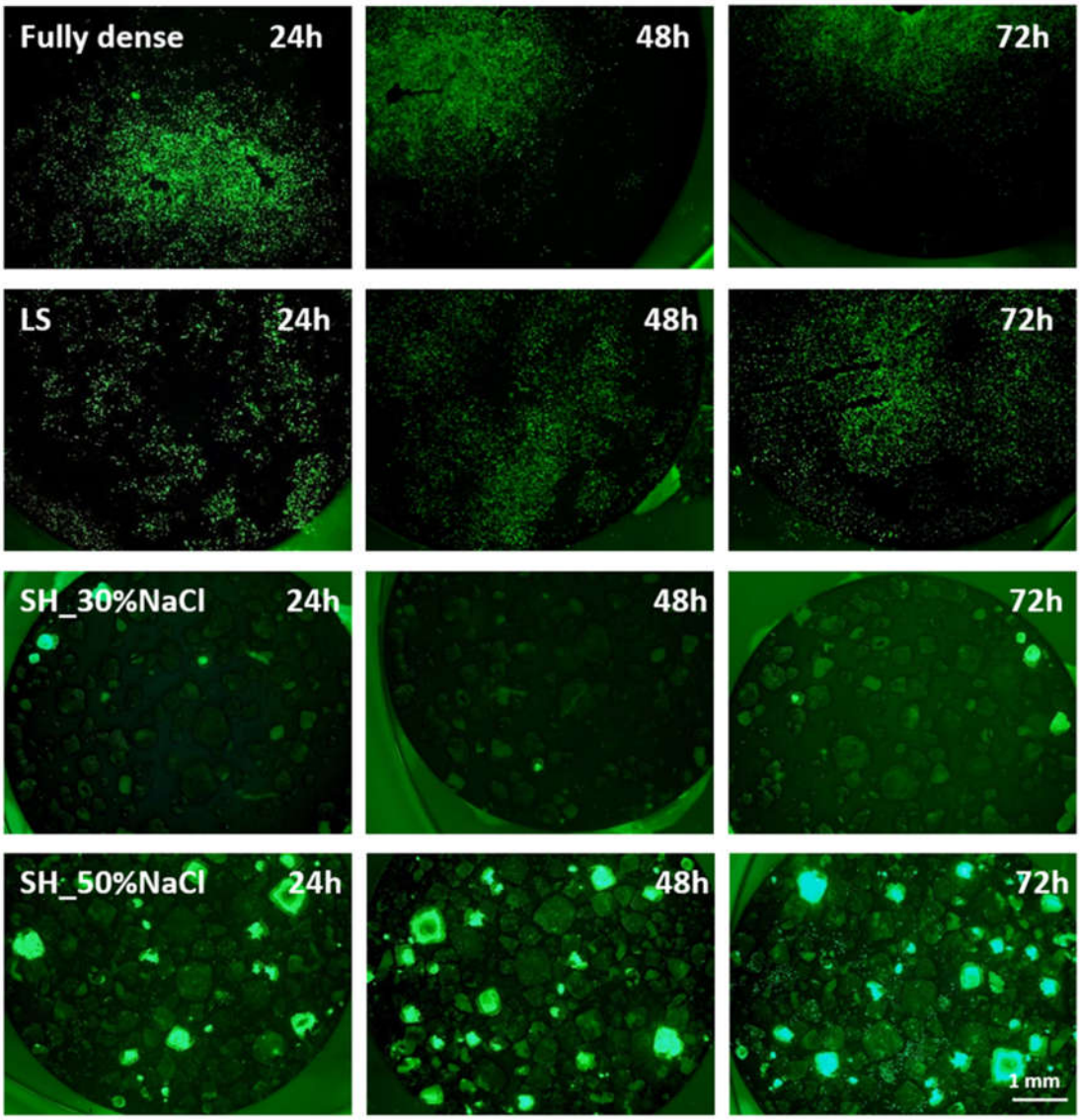

Figure 3. Inverted fluorescence micrographs of C2C12-GFP cells seeded onto fully dense and porous titanium samples fabricated by LS and SH using NaCl spacer particles at 24, 48 and 72 h. An increase in cell attachment is observed in LS and SH_50%NaCl over the entire surface which contrasts to the cells just located at the center of fully dense samples, confirming lower cell migration at 72 h.

Figure 4 showed, at higher magnification, images of C2C12-GFP cells growing at 24, 48 and 72 h of cell incubation. These images corroborate the cell behavior described above and point out the differences between pores and flat surfaces. All porous substrates presented higher surface contact area due to the porosity designed compared to non-porous control samples. Indeed, 50% of total porosity surfaces showed higher cell attachment and cell migration compared to lower porosity levels, 30%, and control Ti surfaces. These factors, roughness and porosity promoted the increased cell adhesion on titanium scaffolds. Moreover, an irregular pore morphology with higher interconnected porosity (P_i) facilitates surface exposure to cells during the adhesion process, as SH_50%NaCl revealed.

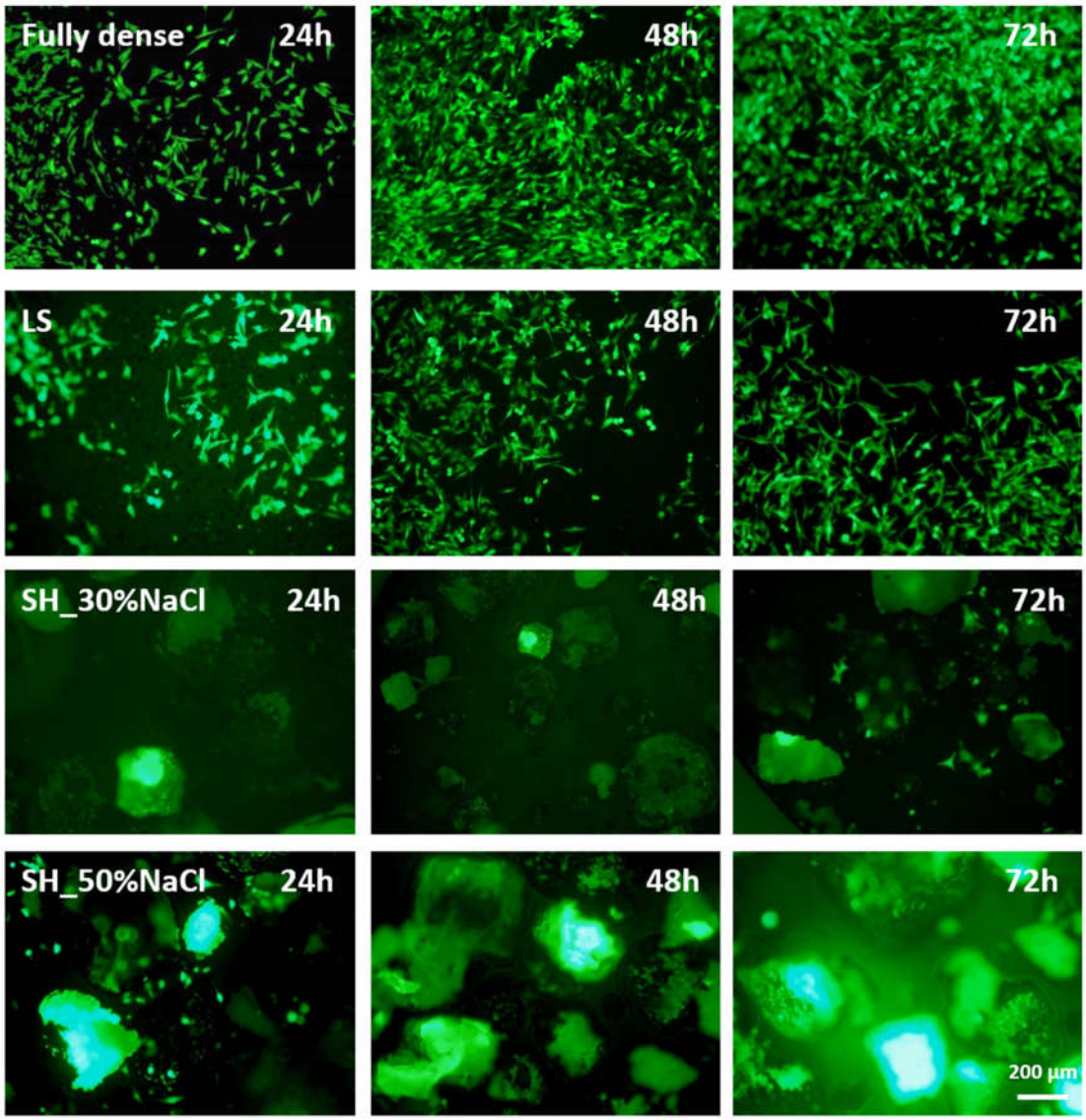

Figure 4. Inverted fluorescence micrographs of C2C12-GFP cells seeded onto fully dense and porous titanium samples fabricated by LS and SH using NaCl spacer particles at 24, 48 and 72 h. An increase of cell adhesion and cell density is observed through the cell incubation time, as expected for cells that are well attached and in a proliferation stage.

It is well-known that the osseointegration process of titanium implants is influenced by the surface properties, the topography and the chemical nature of the material. This osseointegration has been improved by the development of rough surfaces or porous substrates, or by implementing bioactive coatings [42–44]. Commercial implants have been subjected to different surface modification treatments to produce rough surfaces using different methods (mechanical, chemical, sol-gel, anodic oxidation, physical and biochemical) described elsewhere [37,45,46]. While porous substrates offer a higher surface contact area, rough surfaces facilitate the cell anchorage and adhesion process. Indeed, many research studies have reported the relationship between roughness (Sa) and cell adhesion [44,45]. In this study, all specimens were polished to a mirror-like surface—reaching Sa values of 0.7 µm on flat surfaces found in fully dense and on porous substrates, while the internal walls of the pores revealed higher Sa values (i.e., 5 µm in SH_50%NH_4NCO_3) [20]. Besides the roughness difference, the pore geometry has an impact on cellular attachment. Under this

premise, SH_50%NaCl presented an extended pore morphology, plus a bigger pore size, which facilitated the entrance and the cellular attachment to pore's wall. Furthermore, samples with low D_{eq} such us LS at both temperatures did not allow for cellular penetration inside the pore reducing the surface area exposed for cellular anchorage. In addition, lower cell adhesion was detected in pores with rounded morphology (i.e., in SH_30%NaCl with 28.4 ± 4.6% and 347 μm (D_{eq}) compared to SH_50%NaCl with 47.9 ± 3% and 392 μm (D_{eq})). This relationship has been reported for porous Ti substrates using NH_4HCO_3 spacer particles. While SH_30%NH_4HCO_3 showed a larger smooth surface area, SH_50%NH_4HCO_3 presented higher roughness values, with a surface full of peaks and valleys of around 10 μm [39]. They showed not only a rough surface inside the pores but also the presence of micropores due to the sintering process which also increases the roughness inside the pores. Moreover, an irregular pore morphology including geometrical features and the presence of some fractures and cracks due to the compaction process and the removal of the spacer particles contributes to the increased roughness (higher Sa values on SH compared to LS).

After a preliminary biocompatibility study of Ti samples, following the cell culture by inverted fluorescence microscopy, the metabolic activity of this murine cell line MC3T3E1 was assessed at 24, 48 and 72 h of cell incubation; see Figure 5.

Both time and type of substrate, showed significant differences at the 0.05 level. According to Tukey's post-hoc test, the 24 h samples did not show statistical differences, and all surfaces behave similarly. At 48 h, this metabolic activity was statistically different when compared to the SH route, fully dense and LS samples. However, LS and fully dense achieved the highest metabolic levels (at 48 h, $p > 0.05$). Moreover, at 72 h, fully dense showed statistical differences to all porous LS and SH substrates, with $p < 0.05$ and $p < 0.01$ respectively.

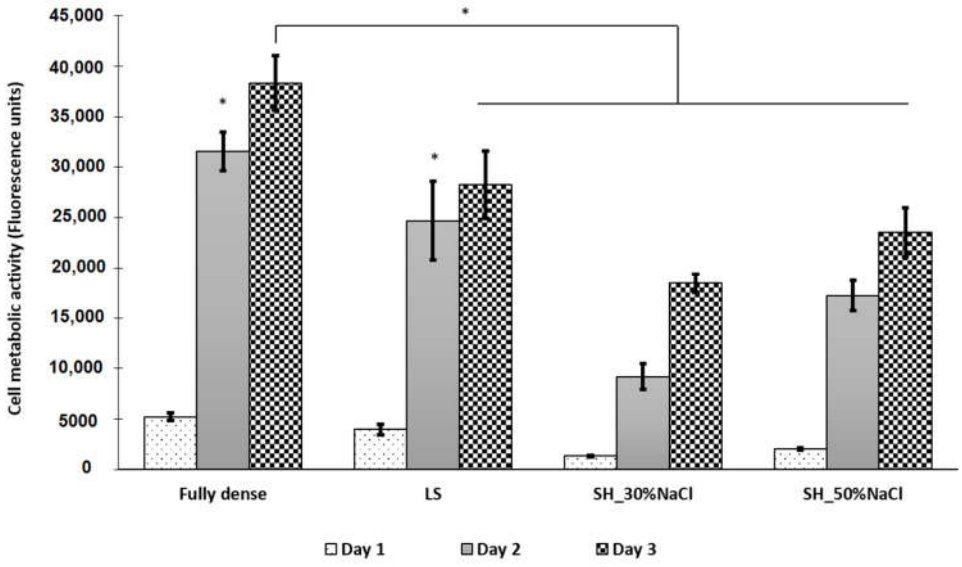

Figure 5. Cell metabolic activity in adhesion and proliferation stages determined by AlamarBlue assay of MC3T3E1 cell line; AlamarBlue results showed a remarkable increased in metabolic activity that belongs to an increase in cell proliferation. Significance level at p value < 0.05 (*).

Although both porous Ti substrates (LS and SH) reached lower cell metabolic activity levels compared to control fully dense for all time points, it has been previously reported that a higher porosity percentage and interconnected porosity leads to cells settle down to the bottom of the tissue culture plate. Thus, a reduced number of cells are able to attach on the sample from the beginning of the experiment [20]. This fact is also observed during the first period of cell incubation using C2C12-

GFP and could explain the lower MC3T3E1 metabolic activity reached in SH porous substrates compared to fully dense and LS at 24 h and 48 h. However, this trend evolved, and the metabolic activity increased reaching in SH_50%NaCl similar metabolic levels to LS with no statistic differences ($p > 0.05$). It should be noticed that the main differences were found in SH_30%NaCl which can be explained by several factors: (1) lower amount of NaCl particles shows lower porosity percentage and a lower interconnected porosity (P_i) which generates samples with lower surface area than 50%; and (2) the D_{eq} is similar to 50%NaCl but the pore morphology (F_f) is more spherical and homogeneous which hinder the cellular attachment to pore walls.

On the other hand, the presence of cellular metabolism confirms the safety of sintering routes to produce biocompatible porous titanium substrates with no residues due to the elimination of spacer particles. These results have been described in previous studies on our research group [47]. In this study, a better in-vitro biological performance was achieved using 50% spacer particles of NH_4HCO_3 compared to other percentages (30%, 40%, 60% and 70%). Indeed, lower cytotoxicity percentages were found for 50% due to the roughness, and pore size and morphology. The two-temperature process in low vacuum of NH_4HCO_3 particles induces higher surface defects, and thus, higher roughness, which affects the cell metabolic activity and adhesion of osteoblast cells [20].

The cellular behavior observed in the flat control sample (fully dense) was similar to those reported in previous studies, in which the metabolic activity during the adhesion process was higher on smooth than the kinetic rough surface [19,20,48]. Cell metabolic activity changes due to the cellular machinery in each step, presenting lower activity for adhesion than for proliferation or differentiation states. Surface roughness has shown the influences on the adhesion and differentiation of osteoblastic cells, thereby reaching a reduction of proliferation rate regarding the higher production of bone matrix proteins, including ALP, collagen, osteopontin and osteocalcin [19,49]. Particularly, other cellular processes such as protein adsorption or hemocompatibility can be improved using surface modification, in bone and vascular tissue regeneration [49,50]. It has been reported that the protein layer deposited onto Ti smooth and Ti rough surfaces is composed of different proteins and different amounts. While Ti smooth surfaces revealed an increasing number of proteins related to glycolysis and apoptosis, proteins related to the cell signaling pathway by integrin and blood coagulation process (Apo E, and antithrombin) were upregulated in rough Ti substrates [50]. Furthermore, Chen and coworkers studied the viability of the osteoblastic cells growing on porous Ti substrates fabricated with sugar as spacer particles, and they did not observe statistical differences between different volume fractions of 30%, 40% and 50% samples [19]. In previous studies in our group, MC3T3 cells achieved lower cell metabolic activity on porous than on flat substrates at 4 and 7 days, but similar responses were found between percentages of the spacer [20]. All these results confirmed the higher cell metabolic levels observed on flat Ti surfaces compared to the levels reached in LS and SH.

Changes in cell shape were also studied as a response to surface topography. Figure 5 shows the evaluation of cell morphologies of the studied specimens. The fully dense surface showed a dense cell monolayer at the center of the sample denoting a reduced cell spreading compared to LS and SH. This delay on cell spreading was in agreement with previous results observed using myoblast cells [20]. However, the increased cell density at the center hindered the analysis of cell cytoskeleton morphology. For that reason, Figure 6 images are presented at the center for all substrates and in the edges and inside the pores of the samples. Cell morphology located at the edge of the fully dense control sample revealed a more rounded cell cytoskeleton which it can be correlated with a more immature cell adhesion state. In contrast, all porous substrates showed an elongated cell morphology and a wider cell cytoskeleton. For instance, LS and SH substrates (30% and 50%) presented flat and pores surfaces that were totally covered and had higher cell density due to the higher surface contact area. Inside the pores, LS had a lower presence of attached MC3T3 than SH substrates, which was noticed by the lower presence of cell nuclei. DAPI staining allowed for the quantification of cell nuclei, confirming higher cell density on SH_50%NaCl compared to FD and LS, as Figure 6C shows.

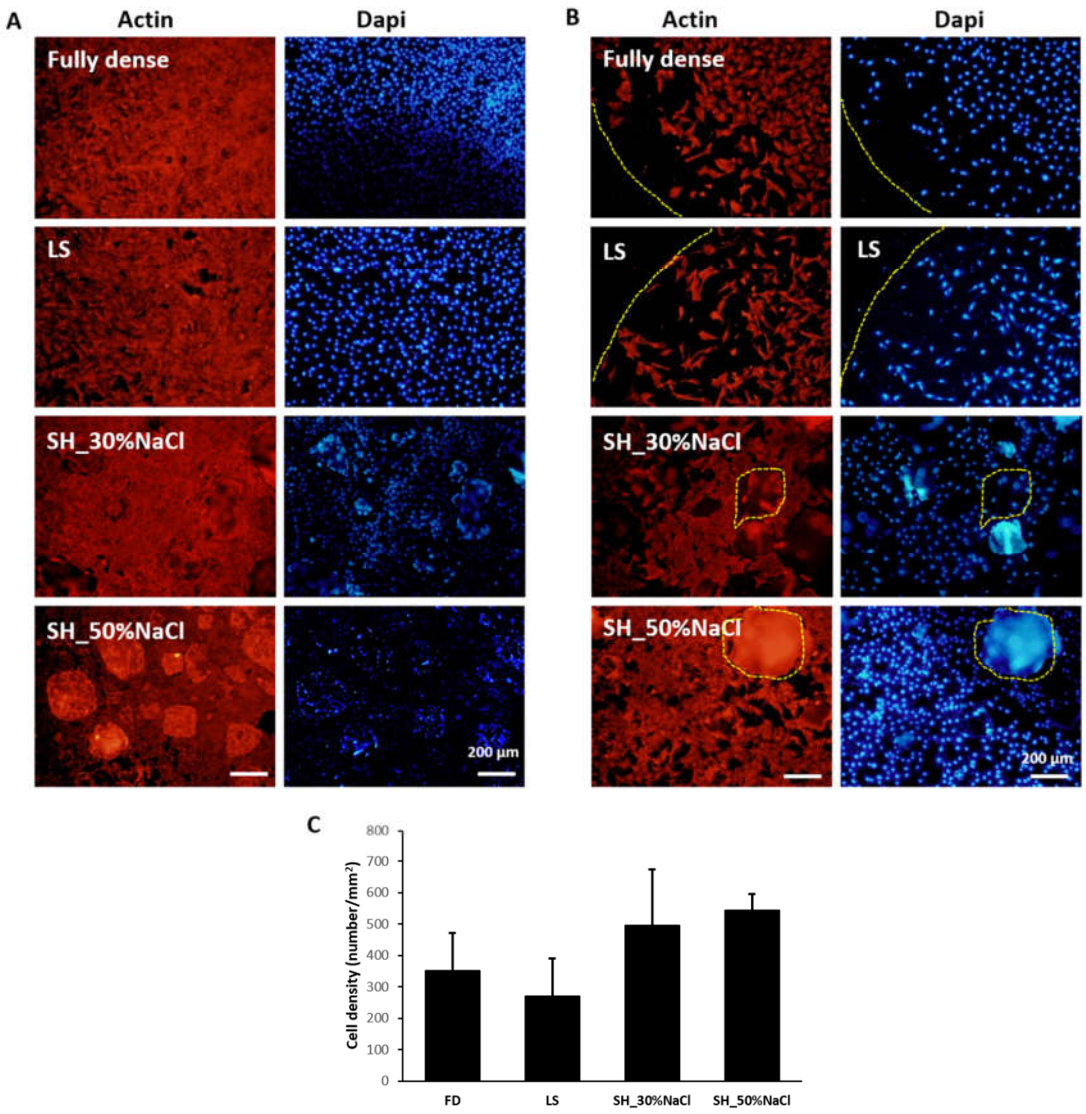

Figure 6. Micrographs of inverted fluorescence microscopy of MC3T3E1 cells seeded onto c.p. fully dense and porous titanium samples fabricated by LS and SH using NaCl spacer particle at 72 h. (**A**) Cell adhesion in the centers of Ti samples. (**B**) Cell adhesion at the edges and inside the pores of Ti substrates. (**C**) Quantification of cell density on each substrate.

These two PM routes offer a higher contact surface compared to fully dense, which it has been reported to promote cytoskeleton development and advanced cell adhesion [20,51]. However, between LS and SH routes, the higher surface exposed inside the pores favored the cell adhesion, as Figure 7 shows by comparing LS with SH_50%NaCl.

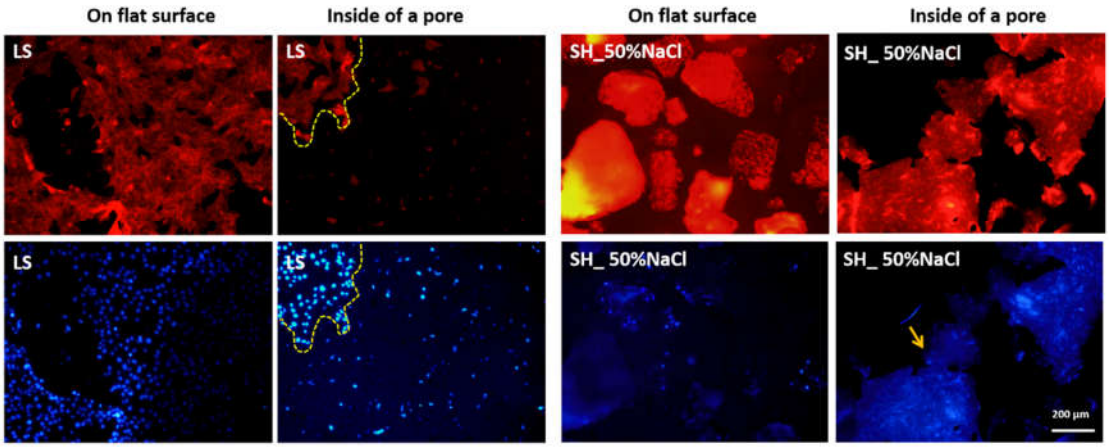

Figure 7. Cell morphology of MC3T3E1 cells growing on LS and SH_50%NaCl scaffolds comparing flat surfaces and inside pores at 72 h of incubation. Images were taken by fluorescent microscopy. Notice an increase of attached cells in SH_50%NaCl inside the pores compared to its flat surface. In contrast, LS presented lower porosity and the preosteoblasts were more abundant on the flat area. Yellow dotted lines and arrows mark the pore edges to indicate the presence of cells attached inside each pore.

In order to further analyze the cell morphology studied on these porous specimens, and to solve the limitations associated with the inverted fluorescence microscope, SEM was performed, and the results are shown in Figure 8. Here, MC3T3E1 cell monolayer was found in all c.p. Ti substrates. Whereas fully dense had an extended cell cytoskeleton at the edges of the sample, the osteoblastic cells were covering the internal walls of pores on porous SH surfaces.

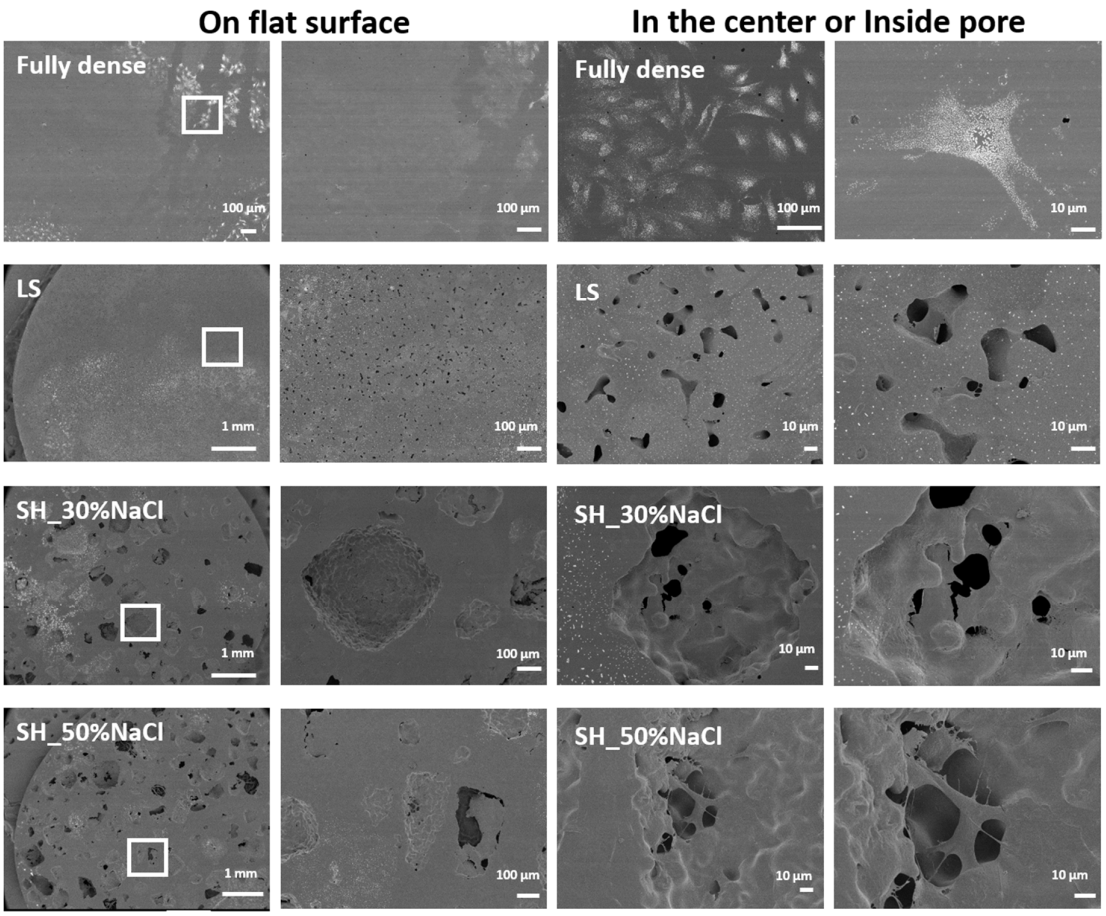

Figure 8. SEM images of MC3T3 E1 cell morphology growing on LS and SH_NaCl surfaces comparing flat surfaces and inside pores at 72 h of incubation.

Furthermore, osteoblasts growing on the control (fully dense) surface presented lower filopodia protrusions which are essential cellular structures during the cell adhesion process. These observations are in agreement with those presented in other studies using MC3T3E1 and SAOS cells [47]. Muñoz and coworkers observed an osteoblastic cell morphology when porous substrates had 50% of the spacer particles [47].

There was a different cell response to higher D_{eq} in SH compared to LS substrates. Higher surface contact area, bigger pore size and a more irregular geometry, facilitated the surface exposed to cell contact which promoted cell interactions reaching an advanced adhesion with the substrate.

SH sintering route, using NaCl and NH_4HCO_3 particles, produces a bigger pore size related to the size of the spacer particle compared to LS, and due to the sintering process and the removal of spacer particles, an increased roughness inside the pores is defined, which also promotes the cell attachment inside the pore. The percentage of spacer particles did not seem to affect cell viability using AlamarBlue (see Figure 9) and MTT [35]; however, the higher amount of spacer particles drives in- pore coalescence, affecting the mechanical properties and its integrity, which finally reduces the implant stability. It is essential to reach a compromise between the mechanical properties of porous implants and biological performance to promote the desired osseointegration [52]. Although multiple factors intervene during bone osseointegration, many studies have reported the relationship between surface roughness, geometry of pores, pore diameter, total and interconnected porosity. The combination of all these factors to reproduce a similar surface to the bone ECM (extracellular matrix) is a great strategy to promote cell differentiation and bone regeneration [33,47,53].

Similarly, these porous substrates were elaborated using a pull of particle sizes without taking into account a specific range. When the spacer particle used to produce porous substrates was sieved before the sample preparation into a limited size, the porosity achieved was more accurate to the percentage designed (see Table 2 for SH_NH_4HCO_3-40%, 100–200 μm and 355–500 μm). These samples offered a similar P_T percentage (40.02% ± 0.6% and 40.08% ± 0.5% for both surfaces), similar density (2.69 ± 0.02 g/cm^3 and 2.67 ± 0.02 g/cm^3) and same enlarged and irregular pore morphology (0.71 ± 0.12 and 0.67 ± 0.06 g/cm^3). The main differences were found in D_{eq} and interconnected porosity, which were superior in SH_NH_4HCO_3-40% (355–500 μm). To analyze the influence of the latter factors, the osteoblast response was studied in longer-term experiments using murine MC3T3E1 cells for 21 days.

Figure 9 shows the results of the metabolic activity of osteoblasts expressed in absorbance, and therefore, their cellular viability. The metabolic activity increases during the period of cellular incubation, reaching optimal values at 21 days, as it has been reported in other studies in which the metabolic activity is greater in differentiation and mineralization stages (14 and 21 days) than in adhesion stages (1–4 days) [20]. There is a greater viability of the osteoblastic cells on SH_NH_4HCO_3-40% (100–200 μm) porous substrates at 21 days of cell culture. Based on the statistic treatment, the cell metabolic activity was significantly different compared to time and samples. At 1, 4, 7 and 14 days all samples showed a similar cellular response in all substrates except in fully dense which showed significant results when compared to 4 days in a fully dense sample. At 21 days the scenario changes, and as pointed out earlier, optimal values were found in porous SH substrates when compared with fully dense and SH_NH_4HCO_3-40% (355–500 μm).

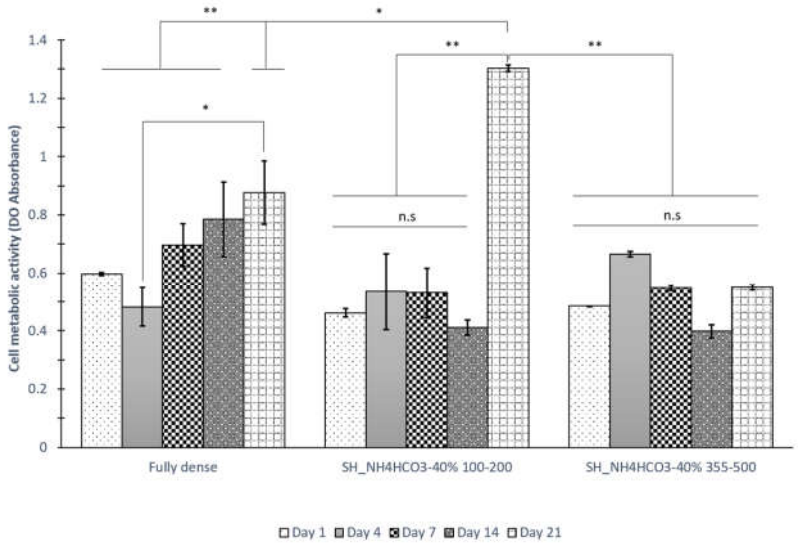

Figure 9. Cell metabolic activity in long proliferation stage (1, 4, 7, 14 and 21 days) determined by AlamarBlue assay of MC3T3E1 cell line; AlamarBlue results showed a remarkable increased in metabolic activity that belongs to an increase in cell proliferation. The p values of < 0.05 (*) and < 0.01 (**) indicate statistical differences, while n.s. indicates a non-significant value.

Regarding the cell metabolism at 14 and 21 days, the metabolic activity is focused on the latter differentiation process, synthesizing a higher increase of proteins and fibers to develop a nutrient extracellular matrix (ECM). The pore size and the percentage of interconnected pores found in these samples offered suitable properties to create a rich bone ECM.

In order to confirm the previous results regarding an increased cell metabolic activity on SH_NH_4HCO_3-40% (100–200 μm) at 21 days, alkaline phosphatase activity (ALP) was evaluated at 4 and 21 days, as Figure 10 shows. At 4 days, osteoblast cells growing on SH_NH_4HCO_3-40% (100–200

μm) achieved similar ALP level to fully dense surfaces, but ALP increased at 21 days on the porous scaffolds and lower enzymatic activity was observed on the fully dense surface.

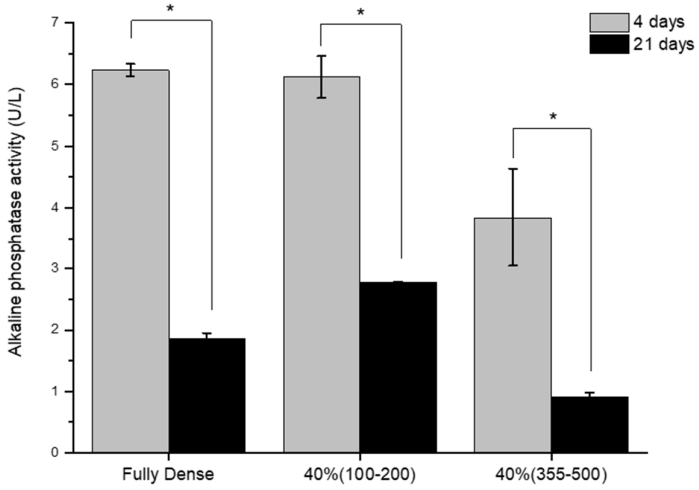

Figure 10. Cell differentiation of osteoblasts on porous scaffolds SH_NH_4HCO_3-40%. In-vitro evaluation of alkaline phosphatase enzyme (ALP) activity measured at 4 and 21 days of cell culture in osteogenic media. Statistical differences are indicated at $p < 0.05$ *.

This increased cell differentiation was contrasted through SEM analysis in all studied specimens. Figure 11 shows the SEM micrographs of osteoblasts growing on Ti substrates. These SEM images showed the osteoblast cell expansion over all surfaces for 7, 14 and 21 days of cell culture. It was observed that osteoblastic cells were well attached and spread onto the surfaces and inside porous in all samples. Detailed observations of the interactions, cell–cell and osteoblasts–surfaces, demonstrated the interconnectivity of the matrix (marked with yellow arrows and asterisks in Figure 11). The cytoplasmatic extensions created bridges across the pores and enlarged filopodia and lamellipodia protrusions which are presented on porous surfaces. The increased cell density on porous samples compared to fully dense ones is remarkable, which at 14 days, still revealed empty areas in the surface with no attached cells. However, at 21 days all surfaces appeared to be completely covered by MC3T3E1 cells (covering pores) and surrounded by bone matrix.

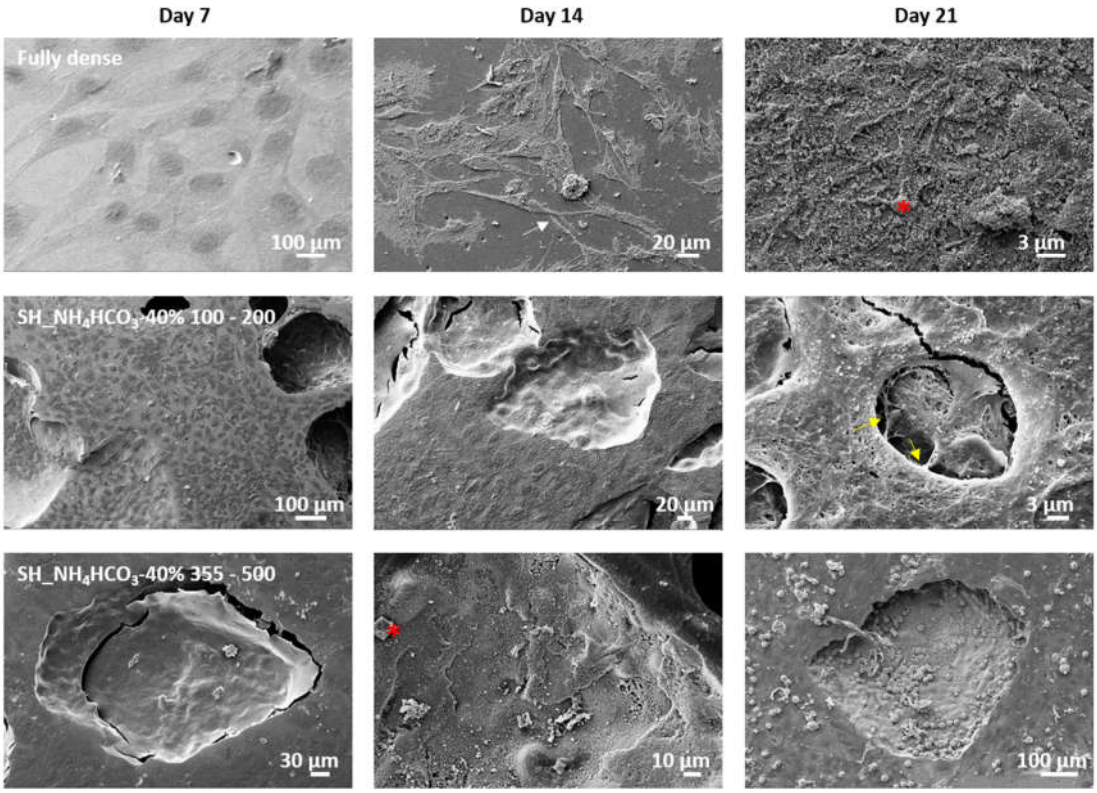

Figure 11. SEM micrographs of the 7, 14 and 21 days of osteoblast culture growing on porous SH_NH_4HCO_3-40%, 100–200 µm and 355–500 µm. Cell morphology and osteoblast proliferation are shown on SH surfaces. The pores covered by osteoblasts at 7 days in SH substrates should be noticed. Cell–cell interaction (white arrow), a cell-surface junction (yellow arrow) and hydroxyapatite (red asterisks) are indicated in the images.

The number of cells detected was greater in the sample of SH_NH_4HCO_3-40% (100–200 µm) since there are pores completely covered by cells at 14 days. The cells adhered through filopodia (fine cellular projections) marked by the white arrow in Figure 11, and lamellipodia (wider extensions), demonstrating the connection with the biomaterial. Fine extensions allowing the cell–cell connection are also distinguished.

From the 14th day of cell culture, the elevated presence of vesicles on the cell surface was highlighted. They are produced by polarized sprouting from the surface of the osteoblast, suggesting the development of a nutrient bone ECM. Many vesicles were observed due to the medium containing β-glycerophosphate (organic phosphate), a substrate of alkaline phosphatase that induces an increase of inorganic phosphates in the medium that will transform into hydroxyapatite marked with a red asterisk in Figure 11 [54,55].

On the 21st day, fully dense Ti and SH_NH_4HCO_3-40% (350–500 µm) discs showed hexagonal structures that suggest a possible nucleation of hydroxyapatite (see Figure 11, red asterisks). In the SH_NH_4HCO_3-40% (100–200 µm) samples, a cell monolayer of mature osteoblast was observed. In previous studies, we have demonstrated that osteoblasts in the samples of 40% space-holder (SH_NH_4HCO_3-40%) were well attached to peaks inside the pores or among depressions, which appear separated by a length that is similar to osteoblast diameter (~20 µm), and the samples with the highest space-holder contents (60 and 70 vol.%) did not show such proper shape of well-attached cells; therefore, the large sizes of pores also could be negative for the osteoblast proliferation [47]. Our results agreed with other authors; they have reported that different ranges of porosity can promote different osteoblast functions. Conway et al. showed that Ti scaffolds with a pore range between 45

and 106 μm presented the best microarchitecture for early stages of osteoblast attachment, whereas a pore size higher than 300 μm exhibited the most favorable conditions for cell proliferation [56].

4. Conclusions

In this study, we have correlated the porosity designed by two different routes, LS and SH, and the mechanical and cellular behavior of porous titanium substrates towards bone osseointegration. In summary, both techniques are simple, economical and easily reproducible for fabricating porous materials as potential substitutes for cortical bone tissue. However, the sizes and contents of the pores obtained using the LS route are insufficient (D_{eq} = 19 μm) to guarantee the bone ingrowth (>100 μm) and to reach appropriate stiffness values (E = 52 GPa versus $E_{Cortical\ bone}$ = 20–25 GPa), while the use of large and heterogeneous (wider populations) spacers compromises the reliability mechanical (σ_y = 180 MPa) of the implant. In-vitro tests show a successful adhesion and spreading of the C2C12-GFP and MC3T3 cell lines (on a flat surface and inside pores of porous samples) confirming the biocompatibility and non-toxicity of both sintering routes. Moreover, both methods enhanced cell adhesion, spreading, proliferation and differentiation of osteoblasts compared to fully dense. However, the use of SH provides bigger pore size, with an irregular pore geometry and higher interconnected porosity, factors that influence cell differentiation of osteoblast. In that sense, SH_NH_4HCO_3-40% (100–200 μm) reached a higher cellular metabolic activity and increased alkaline phosphatase levels at 21 days compared to fully dense and SH_NH_4HCO_3-40% (355–500 μm). In this context, the substrates obtained with 40 vol.% NH_4HCO_3 and ranges size of 100–200 μm, are those that offer suitable biomechanics (E = 45.3 GPa and σ_y = 235 MPa) and biofunctional behavior balance to promote in-vitro osseointegration and solve the stress shielding phenomenon, key factors for the improvement of clinical success of titanium implants.

Author Contributions: Conceptualization, project administration, supervision and methodology, M.-J.M.-G., J.P.A. and Y.T.; investigation, formal analysis and validation A.C., M.G., P.T., S.L., C.A. and M.Á.V.; discussion and writing—original draft preparation, all the authors. All authors have read and agreed to the published version of the manuscript.

Funding: This research was funded by the regional government from Andalusia through FEDER-Junta de Andalucía Research Project, reference US-1259771 (modeling and implementation of the freeze casting technique: gradients of porosity with a tribomechanical equilibrium and electro-stimulated cellular behavior).

Acknowledgments: The authors thank to laboratory technicians Jesus Pinto and Mercedes Sánchez for their technical support and the Tissue Engineering Group (TEG) from University Complutense of Madrid (UCM) for kindly providing the cell line C2C12-GFP.

Conflicts of Interest: The authors declare no conflict of interest.

References

1. Brunette, D.M.; Tengvall, P.; Textor, M.; Thomsen, P. *Titanium in Medicine: Materials Science, Surface Science, Engineering, Biological Responses and Medical Applications*; Springer: Berlin, German, 2001.
2. Van-Noort, R. Titanium: The implant material of today. *J. Mater. Sci.* **1987**, *22*, 3801.
3. Williams, D.F. On the mechanism of biocompatibility. *Biomaterials* **2008**, *29*, 1–13.
4. He, G.; Liu, P.; Tan, Q. Porous titanium materials with entangled wire structure for load-bearing biomedical applications. *J. Mech. Behav. Biomed. Mater.* **2012**, *5*, 16–31.
5. Dizlek, M.E.; Guden, M.; Turkan, U.; Tasdemirci, A. Processing and compression testing of Ti6Al4V foams for biomedical applications. *J. Mater. Sci.* **2009**, *44*, 1512.
6. Zhao, X.; Sun, H.; Lan, L.; Huang, J.; Zhang, H.; Wang, Y. Pore structures of high-porosity NiTi alloys made from elemental powders with NaCl temporary space-holders. *Mater. Lett.* **2009**, *63*, 2402.
7. Ryan, G.E.; Pandit, A.S.; Apatsidis, D.P. Fabrications Methods of porous metals for use in orthopaedic applications. *Biomaterials* **2006**, *27*, 2651–2670.
8. Bram, M.; Stiller, C.; Buchkremer, H.P.; Stover, D.; Baur, H. High-porosity titanium, stainless steel, and superalloy parts. *Adv. Eng. Mater.* **2000**, *2*, 196–199.
9. Dunand, D.C. Processing of titanium foams. *Adv. Eng. Mater.* **2004**, *6*, 369–376.

10. Wen, C.E.; Yamada, Y.; Shimojima, K.; Chino, Y.; Asahina, T.; Mabuchi, M. Processing and Mechanical Properties of Autogenous Titanium Implant Materials. *Mater. Sci. Mater. Med.* **2002**, *13*, 397–401.
11. Singh, R.; Lee, P.D.; Dashwood, R.J.; Lindley, T.C. Titanium foams for biomedical applications: a review. *Mater. Technol.* **2010**, *25*, 127–136.
12. Niinomi, M.; Nakai, M.; Hieda, J. Development of new metallic alloys for biomedical applications. *Acta. Biomater.* **2012**, *8*, 3888–3903.
13. Gepreel, M.A.-H.; Niinomi, M. Biocompatibility of Ti-alloys for long-term implantation. *J. Mech. Behav. Biomed. Mater.* **2013**, *20*, 407–415.
14. Stamboulis, A.G.; Boccaccini, A.R.; Hench, L.L. Novel biodegradable polymer/bioactive glass composites for tissue engineering applications. *Adv. Eng. Mater.* **2002**, *4*, 105–109.
15. Domínguez-Trujillo, C.; Ternero, F.; Rodríguez-Ortiz, J.A.; Heise, S.; Boccaccini, A.R.; Lebrato, J.; Torres, Y. Bioactive coatings on porous titanium for biomedical applications. *Surf. Coat. Tech.* **2018**, *349*, 584–592.
16. Hsu, H.-C.; Hsu, S.-K.; Wu, S.-C.; Wang, P.-H.; Ho, W.-F. Design and characterization of highly porous titanium foams with bioactive surface sintering in air. *J. Alloys Compd.* **2013**, *575*, 326–332.
17. Ye, B.; Dunand, D.C. Titanium foams produced by solid-state replication of NaCl powders. *Mater. Sci. Eng., A* **2010**, *528*, 691–697, doi:10.1016/j.msea.2010.09.054.
18. Li, J.; Jansen, J.A.; Walboomers, X.F.; van den Beucken, J.J. Mechanical aspects of dental implants and osseointegration: A narrative review. *J. Mech. Behav. Biomed. Mater.* **2019**, *103*, 103574.
19. Chen, Y.; Frith, J.E.; Dehghan-Manshadi, A.; Kent, D.; Bermingham, M.; Dargusch, M. Biocompatible porous titanium scaffolds produced using a novel space holder technique. *J. Biomed. Mater. Res. Part B* **2018**, *106*, 2796–2806.
20. Civantos, A.; Domínguez, C.; Pino, R.J.; Setti, G.; Pavon, J.J.; Martínez-Campos, E.; Garcia, F.J.G.; Rodriguez, J.A.; Allain, J.P.; Torres, Y. Designing bioactive porous titanium interfaces to balance mechanical properties and in vitro cells behavior towards increased osseointegration. *Surf. Coat. Technol.* **2019**, *368*, 162–174.
21. Schmidutz, F.; Agarwal, Y.; Müller, P.; Gueorguiev, B.; Richards, R.; Sprecher, C. Stress-shielding induced bone remodeling in cementless shoulder resurfacing arthroplasty: a finite element analysis and in vivo results. *J. Biomech.* **2014**, *47*, 3509–3516.
22. Dabrowski, B.; Swieszkowski, W.; Godlinski, D.; Kurzydlowski, K.J. Highly porous titanium scaffolds for orthopaedic applications. *J. Mech. Behav. Biomed. Mater. B: Appl. Biomater.* **2010**, *95*, 53–61.
23. Herrera, A.; Yánez, A.; Martel, O.; Afonso, H.; Monopoli, D. Computational study and experimental validation of porous structures fabricated by electron beam melting: A challenge to avoid stress shielding. *Mater. Sci. Eng. C* **2014**, *45*, 89–93.
24. Muñoz, S.; Castillo, S.; Torres, Y. Different models for simulation of mechanical behaviour of porous materials. *J. Mech. Behav. Biomed. Mater.* **2018**, *80*, 88–96.
25. Arabnejad, S.; Johnston, B.; Tanzer, M.; Pasini, D. Fully porous 3D printed titanium femoral stem to reduce stress-shielding following total hip arthroplasty. *J. Orthop. Res.* **2017**, *35*, 1774–1783.
26. Lascano, S.; Arévalo, C.; Montealegre-Melendez, I.; Muñoz, S.; Rodriguez-Ortiz, J.A.; Trueba, P.; Torres, Y. Porous Titanium for Biomedical Applications: Evaluation of the Conventional Powder Metallurgy Frontier and Space-Holder Technique. *Appl. Sci.* **2019**, *9*, 982.
27. Pavón, J.J.; Trueba, P.; Rodríguez-Ortiz, J.A.; Torres, Y. Development of new titanium implants with longitudinal gradient porosity by space-holder technique. *J. Mater. Sci.* **2015**, *50*, 6103–6112.
28. Miao, X.; Sun, D. Graded/Gradient Porous Biomaterials. *Materials* **2010**, *3*, 26–47.
29. Torres, Y.; Lascano, S.; Bris, J.; Pavón, J.; Rodriguez, J.A. Development of porous titanium for biomedical applications: A comparison between loose sintering and space-holder techniques. *Mater. Sci. Eng. C* **2014**, *37*, 148–155, doi:10.1016/j.msec.2013.11.036.
30. Subramani, K.; Mathew, R.T.; Pachauri, P. Titanium surface modification techniques for dental implants—from microscale to nanoscale. In *Emerging Nanotechnologies in Dentistry*; Elsevier: Amsterdam, The Netherlands, 2018; pp. 99–124.
31. Domínguez-Trujillo, C.; Ternero, F.; Rodríguez-Ortiz, J.A.; Pavón, J.J.; Montealegre-Meléndez, I.; Arévalo, C.; García-Moreno, F.; Torres, Y. Improvement of the balance between a reduced stress shielding and bone ingrowth by bioactive coatings onto porous titanium substrates. *Surf. Coat. Technol.* **2018**, *338*, 32–37.

32. Domínguez-Trujillo, C.; Beltrán, A.M.; Garvi, M.D.; Salazar-Moya, A.; Lebrato, J.; Hickey, D.J.; Rodríguez-Ortiz, J.A.; Kamm, P.H.; Lebrato, C.; García-Moreno, F. Bacterial behavior on coated porous titanium substrates for biomedical applications. *Surf. Coat. Technol.* **2019**, *357*, 896–902.
33. Takemoto, M.; Fujibayashi, S.; Neo, M.; So, K.; Akiyama, N.; Matsushita, T.; Kokubo, T.; Nakamura, T. A porous bioactive titanium implant for spinal interbody fusion: an experimental study using a canine model. *J. Neurosurg. Spine.* **2007**, *7*, 435.
34. Scislowska-Czarnecka, A.; Menaszek, E.; Szaraniec, B.; Kolaczkowska, E. Ceramic modifications of porous titanium: effects on macrophage activation. *Tissue Cell* **2012**, *44*, 391–400.
35. Borjas, S.; Gil, E.J.; Cordero, L.; Pavón, J.J.; Rodriguez-Ortiz, J.A.; Boccaccini, A.R.; Torres, Y. Electrophoretic deposition and characterization of chitosan/45S5 bioactive glass composite coatings on porous titanium for biomedical applications. *Key Eng. Mater*. **2015**, 654, 189–194.
36. Tobin, E.J. Recent coating developments for combination devices in orthopedic and dental applications: a literature review. *Adv. Drug Deliv. Rev.* **2017**, *112*, 88–100.
37. Civantos, A.; Allain, J.P.; Pavón, J.J.; Shetty, A.; El-Atwani, O.; Walker, E.; Arias, S.L.; Gordon, E.; Rodríguez-Ortiz, J.A.; Chen, M., et al. Directed Irradiation Synthesis as an Advanced Plasma Technology for Surface Modification to Activate Porous and "as-received" Titanium Surfaces. *Metals* **2019**, *9*, 1349.
38. Wang, M.; Tang, T. Surface treatment strategies to combat implant-related infection from the beginning. *J. Orthop. Transl.* **2019**, *17*, 42–54.
39. Torres, Y.; Pavón, J.; Rodríguez, J. Processing and characterization of porous titanium for implants by using NaCl as space holder. *J. Mater. Process. Technol.* **2012**, *212*, 1061–1069.
40. Torres, Y.; Rodríguez, J.A.; Arias, S.; Echeverry, M.; Robledo, S.; Amigó, V.; Pavón, J.J. Processing, Characterization and biological testing of porous titanium obtained by space-holder technique. *J. Mater. Sci.* **2012**, *47*, 6565–6576.
41. Kikuchi, M.; Takahashi, M.; Okuno, O. Elastic moduli of cast Ti–Au, Ti–Ag, and Ti–Cu alloys. *Dent. Mater.* **2006**, *22*, 641–646.
42. Schwarz, M.L.; Kowarsch, M.; Rose, S.; Becker, K.; Lenz, T.; Jani, L. Effect of surface roughness, porosity, and a resorbable calcium phosphate coating on osseointegration of titanium in a minipig model. *J. Biomed. Mater. Res. A* **2009**, *89*, 667–678.
43. Le Guéhennec, L.; Soueidan, A.; Layrolle, P.; Amouriq, Y. Surface treatments of titanium dental implants for rapid osseointegration. *Dent Mater.* **2007**, *23*, 844–854.
44. Civantos, A.; Martinez-Campos, E.; Ramos, V.; Elvira, C.; Gallardo, A.; Abarrategi, A. Titanium coatings and surface modifications: toward clinically useful bioactive implants. *ACS Biomater. Sci Eng.* **2017**, *3*, 1245–1261.
45. Martin, J.; Dean, D.D.; Cochran, D.L.; Simpson, J.; Boyan, B.; Schwartz, Z. Proliferation, differentiation, and protein synthesis of human osteoblast-like cells (MG63) cultured on previously used titanium surfaces. *Clin Oral Implants Res.* **1996**, *7*, 27–37.
46. Izman, S.; Abdul-Kadir, M.R.; Anwar, M.; Nazim, E.; Rosliza, R.; Shah, A.; Hassan, M. Surface Modification Techniques for Biomedical Grade of Titanium Alloys: Oxidation, Carburization and Ion Implantation Processes. In *Titanium Alloys–Towards Achieving Enhanced Properties for Diversified Applications*; Nurul Amin, A.K.M., Ed.; Books on Demand: Rijeka, Croatia, 2012; pp. 201–228.
47. Muñoz, S.; Pavón, J.; Rodríguez-Ortiz, J.A.; Civantos, A.; Allain, J.P.; Torres, Y. On the influence of space holder in the development of porous titanium implants: Mechanical, computational and biological evaluation. *Mater. Charact.* **2015**, *108*, 68–78.
48. do Prado, R.F.; de Oliveira, F.S.; Nascimento, R.D.; de Vasconcellos, L.M.R.; Carvalho, Y.R.; Cairo, C.A.A. Osteoblast response to porous titanium and biomimetic surface: In vitro analysis. *Mater. Sci. Eng. C* **2015**, *52*, 194–203.
49. Li, G.; Wang, L.; Pan, W.; Yang, F.; Jiang, W.; Wu, X.; Kong, X.; Dai, K.; Hao, Y. In vitro and in vivo study of additive manufactured porous Ti6Al4V scaffolds for repairing bone defects. *Sci. Rep.* **2016**, *6*, 34072.
50. Romero-Gavilan, F.; Sánchez-Pérez, A.M.; Araújo-Gomes, N.; Azkargorta, M.; Iloro, I.; Elortza, F.; Gurruchaga, M.; Goñi, I.; Suay, J. Proteomic analysis of silica hybrid sol-gel coatings: a potential tool for predicting the biocompatibility of implants in vivo. *Biofouling* **2017**, *33*, 676–689.
51. Vilardell, A.; Cinca, N.; Garcia-Giralt, N.; Dosta, S.; Cano, I.; Nogués, X.; Guilemany, J. Osteoblastic cell response on high-rough titanium coatings by cold spray. *J. Mater. Sci. Mater. Med.* **2018**, *29*, 19.

52. Caparros, C.; Guillem-Martí, J.; Molmeneu, M.; Punset, M.; Calero, J.; Gil, F. Mechanical properties and in vitro biological response to porous titanium alloys prepared for use in intervertebral implants. *J. Mech. Behav. Biomed. Mater.* **2014**, *39*, 79–86.
53. Otsuki, B.; Takemoto, M.; Fujibayashi, S.; Neo, M.; Kokubo, T.; Nakamura, T. Pore throat size and connectivity determine bone and tissue ingrowth into porous implants: three-dimensional micro-CT based structural analyses of porous bioactive titanium implants. *Biomaterials* **2006**, *27*, 5892–5900.
54. Anderson, H.C. Molecular biology of matrix vesicles. *Clin. Orthop. Relat. Res.* **1995**, 266–280.
55. Anderson, H.C.; Garimella, R.; Tague, S.E. The role of matrix vesicles in growth plate development and biomineralization. *Front. Biosci.* **2005**, *10*, 822–837.
56. Torres-Sanchez, C.; Al Mushref, F.; Norrito, M.; Yendall, K.; Liu, Y.; Conway, P.P. The effect of pore size and porosity on mechanical properties and biological response of porous titanium scaffolds. *Mater. Sci. Eng., C* **2017**, *77*, 219–228.